nature physics

LETTERS

https://doi.org/10.1038/s41567-019-0450-7

Discrepancy between experimental and theoretical β-decay rates resolved from first principles

P. Gysbers[1,2], G. Hagen[3,4]*, J. D. Holt[1], G. R. Jansen[3,5], T. D. Morris[3,4,6], P. Navrátil[1], T. Papenbrock[3,4], S. Quaglioni[7], A. Schwenk[8,9,10], S. R. Stroberg[1,11,12] and K. A. Wendt[7]

The dominant decay mode of atomic nuclei is beta decay (β-decay), a process that changes a neutron into a proton (and vice versa). This decay offers a window to physics beyond the standard model, and is at the heart of microphysical processes in stellar explosions and element synthesis in the Universe[1–3]. However, observed β-decay rates in nuclei have been found to be systematically smaller than for free neutrons: this 50-year-old puzzle about the apparent quenching of the fundamental coupling constant by a factor of about 0.75 (ref. [4]) is without a first-principles theoretical explanation. Here, we demonstrate that this quenching arises to a large extent from the coupling of the weak force to two nucleons as well as from strong correlations in the nucleus. We present state-of-the-art computations of β-decays from light- and medium-mass nuclei to ^{100}Sn by combining effective field theories of the strong and weak forces[5] with powerful quantum many-body techniques[6–8]. Our results are consistent with experimental data and have implications for heavy element synthesis in neutron star mergers[9–11] and predictions for the neutrino-less double-β-decay[3], where an analogous quenching puzzle is a source of uncertainty in extracting the neutrino mass scale[12].

Gamow–Teller transitions are a form of β-decay in which the spins of the β-neutrino pair emitted during the nuclear decay are aligned. Remarkably, calculated Gamow–Teller strengths appear to reproduce most of the experimental data if the fundamental constant $g_A \approx 1.27$ characterizing the coupling of the weak interaction to a nucleon is quenched by a factor of $q \approx 0.75$ (refs. [13–16]). Missing nuclear correlations (that is, a lack of complexity in nuclear wavefunctions due to the limitations of nuclear models) as well as neglected contributions from meson-exchange currents (that is, coupling of the weak force to two nucleons) have been proposed as possible causes of the quenching phenomenon[4]. However, a solution has so far remained elusive. To address the quenching puzzle, we carry out a comprehensive study of Gamow–Teller decays through many-body computations of nuclei based on effective field theories (EFTs) of quantum chromodynamics[5,17], including an unprecedented amount of correlations in the nuclear wavefunctions. The EFT approach offers the prospect of accuracy, by encoding the excluded high-energy physics through coefficients adjusted to the data, and precision, from the systematically improvable EFT expansion. Moreover, EFT enables a consistent description of the coupling of weak interactions to two nucleons via two-body currents (2BCs). In the EFT approach, 2BCs enter as subleading corrections to the one-body standard Gamow–Teller operator $\sigma\tau^+$ (with Pauli spin and isospin matrices σ and τ, respectively); they are smaller but significant corrections to weak transitions as three-nucleon forces are smaller but significant corrections to the nuclear interaction[5,17].

In this work we focus on strong Gamow–Teller transitions, where the effects of quenching should dominate over cancellations due to fine details (as occur in the famous case of the ^{14}C decay used for radiocarbon dating[18,19]). An excellent example is the super-allowed β-decay of the doubly magic ^{100}Sn nucleus (Fig. 1), which exhibits the strongest Gamow–Teller strength so far measured in all atomic nuclei[20]. A first-principles description of this exotic decay, in such a heavy nucleus, presents a significant computational challenge. However, its equal 'magic' numbers ($Z = N = 50$) of protons and neutrons arranged into complete shells makes ^{100}Sn an ideal candidate for large-scale coupled-cluster calculations[21], while the daughter nucleus ^{100}In can be reached via novel extensions of the high-order charge-exchange coupled-cluster methods developed in this work (see Methods and Supplementary Figs. 4, 12 and 15 for details). This method includes correlations via a vast number of particle–hole excitations of a reference state and also employs 2BCs in the transition operator.

Figure 1 shows our results for the strength (that is, the absolute square of the transition matrix element, M_{GT}) of the Gamow–Teller transition to the dominant $J^\pi = 1^+$ state in the ^{100}In daughter nucleus (see Supplementary Table 1 and Supplementary Fig. 12 for more details). To investigate systematic trends and sensitivities to the nuclear Hamiltonian, we employed a family of established EFT interactions and corresponding currents[22–24]. For increased precision, we also developed a new interaction labelled NN-N^{4}LO + 3N$_{\mathrm{lnl}}$ which is constrained to reproduce the triton half-life (see Methods for details on the Hamiltonians considered). The open symbols in Fig. 1 depict the decay with the standard, leading-order coupling of the weak force to a single nucleon in the non-relativistic limit (that is, via the standard Gamow–Teller operator $\sigma\tau^+$). The differences with respect to the extreme single-particle model (ESPM), which

[1]TRIUMF, Vancouver, British Columbia, Canada. [2]Department of Physics and Astronomy, University of British Columbia, Vancouver, British Columbia, Canada. [3]Physics Division, Oak Ridge National Laboratory, Oak Ridge, TN, USA. [4]Department of Physics and Astronomy, University of Tennessee, Knoxville, TN, USA. [5]National Center for Computational Sciences, Oak Ridge National Laboratory, Oak Ridge, TN, USA. [6]Computational Sciences and Engineering Division, Oak Ridge National Laboratory, Oak Ridge, TN, USA. [7]Nuclear and Chemical Science Division, Lawrence Livermore National Laboratory, Livermore, CA, USA. [8]Institut für Kernphysik, Technische Universität Darmstadt, Darmstadt, Germany. [9]ExtreMe Matter Institute EMMI, GSI Helmholtzzentrum für Schwerionenforschung GmbH, Darmstadt, Germany. [10]Max-Planck-Institut für Kernphysik, Heidelberg, Germany. [11]Physics Department, Reed College, Portland, OR, USA. [12]Department of Physics, University of Washington, Seattle, WA, USA. *e-mail: hageng@ornl.gov

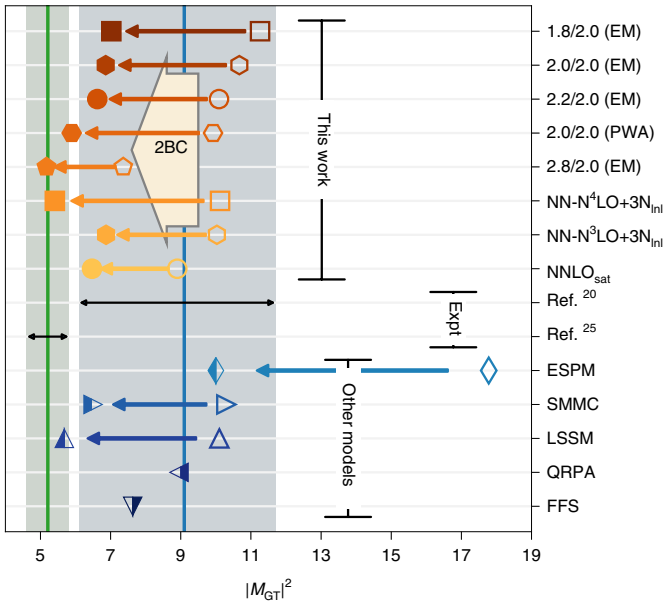

Fig. 1 | Gamow–Teller strength in ^{100}Sn. Comparison of the Gamow–Teller strength $|M_{GT}|^2$ for the β-decay of ^{100}Sn calculated in this work compared to data[20], systematics[25] and other models (extreme single-particle model (ESPM), shell-model Monte-Carlo (SMMC), large-space shell-model (LSSM), quasiparticle random-phase approximation (QRPA) and finite Fermi systems (FFS)) from ref. [20]. Open symbols represent results obtained with the standard Gamow–Teller operator ($\sigma\tau$), filled symbols also include two-body currents (2BCs) and partially filled symbols show values following from the multiplication of the computed Gamow–Teller strength by the square of a phenomenological quenching factor. Each of our ^{100}Sn calculations carries a conservatively estimated uncertainty of about 10% (not shown to avoid overcrowding the figure).

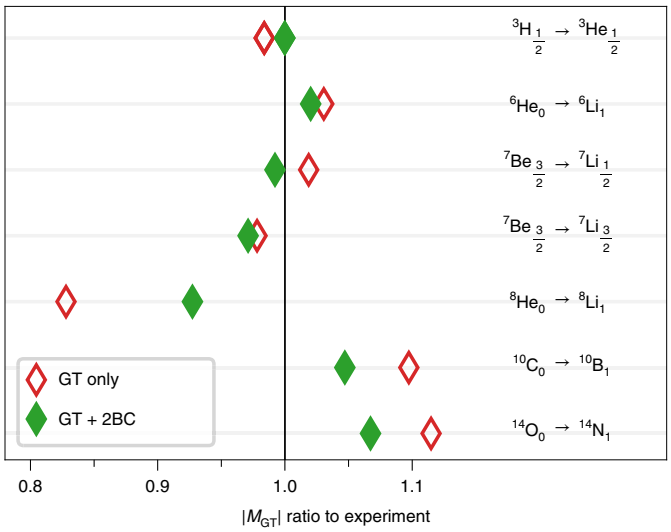

Fig. 2 | Gamow–Teller strengths in light nuclei. Theory-to-experiment ratio for the Gamow–Teller matrix elements of six strong transitions in light nuclei for the NN-N^{4}LO + 3N$_{lnl}$ interaction developed in this work. The subscripts in the legend denote the total angular momenta of the parent and daughter states. All initial states are ground states. In the case of ^{3}H → ^{3}He, ^{6}He → ^{6}Li and ^{7}Be → ^{7}Li$_{\frac{3}{2}}$, the daughter nucleus is in its ground state, while the ^{7}Be → ^{7}Li$_{\frac{1}{2}}$, ^{8}He → ^{8}Li$_1$ and ^{10}C → ^{10}B$_1$ are decays to the first excited state of the daughter nucleus, and the ^{14}O → ^{14}N$_1$ is a decay to the second excited state of ^{14}N. Open symbols correspond to results obtained with the standard Gamow–Teller $\sigma\tau$ operator, and full symbols include 2BCs. The results are converged to within 3% with respect to the model-space size. This uncertainty is slightly larger than the marker size and is not shown for transparency.

approximates both ^{100}Sn and its ^{100}In daughter as a single shell-model configuration, reveals the influence of correlations among the nucleons. The full symbols include 2BCs, using consistent couplings as in the employed EFT interactions. Finally, the partially filled symbols in Fig. 1 represent results from other models from ref. [20], where the standard Gamow–Teller operator has been multiplied by a quenching factor of $q \approx 0.75$.

Based on the results shown in Fig. 1, we predict the range $5.2(5) \lesssim |M_{GT}|^2 \lesssim 7.0(7)$ for the Gamow–Teller strength. This range overlaps with the evaluation in ref. [25], based on systematic experimental trends in tin isotopes, and the lower end of the measurement in ref. [20]. The quenching factor we obtain from 2BCs depends somewhat on the employed Hamiltonian and is in the range $q_{2BC} = 0.73$–0.85. This range is consistent with the value $q = 0.75(2)$ from ref. [25]. In the present work we used the spread of results obtained with the selected set of EFT interactions and 2BCs as an estimate of the systematic uncertainty. A more thorough quantification of the uncertainties associated with the many-body methods and EFT truncations is beyond the scope of this work, and will be addressed in future studies. We note that neglected higher-order correlations in our coupled-cluster approach will further reduce the Gamow–Teller strength (see Supplementary Information for details).

Moreover, we observe that the spread for the ^{100}Sn Gamow–Teller strength obtained for the family of EFT interactions used here is significantly reduced (by a factor two) when 2BCs are included. This is consistent with ideas from EFT that the residual cutoff dependence is due to neglected higher-order terms in the Hamiltonian and 2BCs. In addition, we find that the relative contributions to the quenching of the Gamow–Teller strength coming from correlations and 2BCs vary as a function of the resolution scale of the underlying EFT interactions.

Starting from the extreme single-particle model, and adding first correlations and then the effects of 2BC, we find that the quenching from correlations typically increases with increasing resolution scale of the interaction, and that most of the quenching stems from correlations. However, adding first the effects of the 2BCs and then the correlations shows that the quenching from 2BCs increases with decreasing resolution scale and that most of the quenching stems from 2BCs for all but the 'hardest' potentials considered in this work (see Supplementary Fig. 6 for details).

For a comprehensive study, we now turn to β-decays of light- and medium-mass nuclei. Using a selection of the EFT interactions and 2BCs adopted for ^{100}Sn, we achieved an overall good description of β-decays in light nuclei. Figure 2 shows theory-to-experiment ratios for large Gamow–Teller transitions in light nuclei. Here, we highlight the results obtained for the high-precision NN-N^{4}LO + 3N$_{lnl}$ interaction and corresponding 2BCs developed in this work. As detailed in the Methods, the 2BCs and three-nucleon forces 3N$_{lnl}$ are parametrized consistently and are constrained to reproduce the empirical value of the triton β-decay half-life. Our calculations were carried out with the no-core shell model (NCSM)[6], a virtually exact treatment of correlations in the nuclear wavefunctions (see Methods for details). The role of 2BCs is relatively small in light nuclei with mass numbers $A \leq 7$. Full nuclear wavefunctions already provide a rather satisfactory description of the transitions with the standard Gamow–Teller operator. Furthermore, the inclusion of 2BCs may enhance (for example, ^{8}He → ^{8}Li), quench (for example, ^{7}Be$_{\frac{3}{2}}$ → ^{7}Li$_{\frac{1}{2}}$), or have virtually no impact on the computed transition (for example, ^{7}Be$_{\frac{3}{2}}$ → ^{7}Li$_{\frac{3}{2}}$; see also Supplementary Fig. 13). The small role

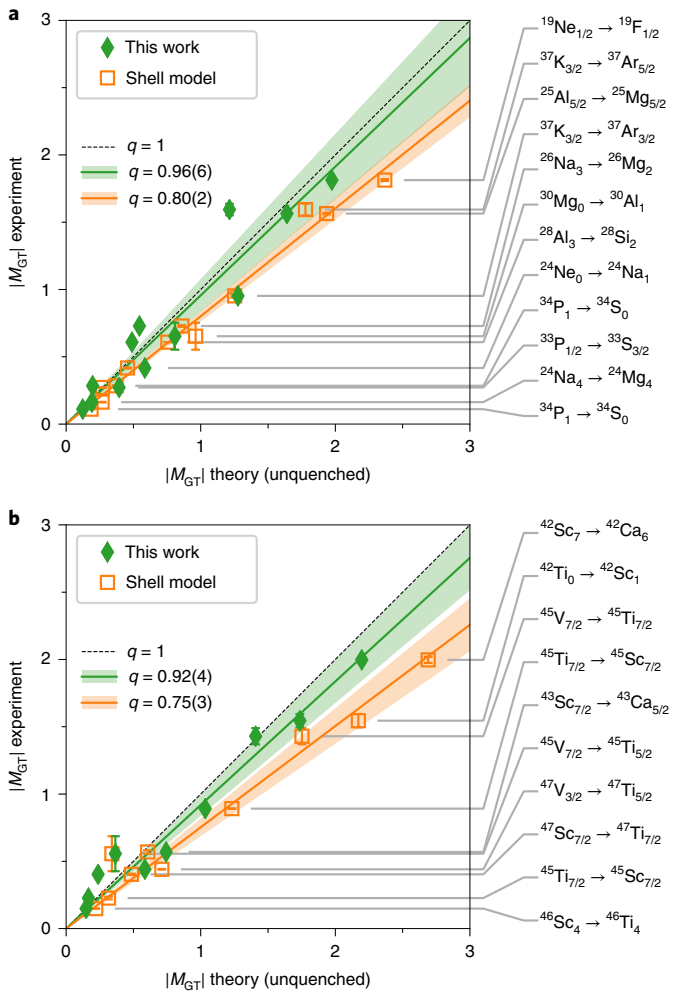

Fig. 3 | Gamow–Teller strengths in medium-mass nuclei. Comparison of experimental[30] and theoretical Gamow–Teller matrix elements for medium-mass nuclei. **a**,**b**, Plots of Gamow–Teller matrix elements: *sd*-shell (**a**) and lower *pf*-shell (**b**). Theoretical results were obtained using phenomenological shell-model interactions[16,31] with an unquenched standard Gamow–Teller $\sigma\tau$ operator (open orange squares), and using the VS-IMSRG approach with the NN-N^{4}LO + 3N$_{\rm lnl}$ interaction and consistently evolved Gamow–Teller operator plus 2BCs (filled green diamonds). The linear fits show the resulting quenching factor q given in the panels, and shaded bands indicate one standard deviation from the average quenching factor. Experimental uncertainties, taken from ref. [30], are shown as vertical error bars.

of 2BCs in $A \leq 7$ nuclei is similar to what was found in the Green's function Monte Carlo calculations of ref.[26]. We find a rather substantial enhancement of the ^{8}He Gamow–Teller matrix element due to the 2BC. Let us mention, though, that this transition matrix element is the smallest of those presented in Fig. 2. We note that, for the other Hamiltonians employed in this work, the 2BCs and 3N were not fit to reproduce the triton half-life; nevertheless, the inclusion of 2BCs for most of these cases also improves the agreement with data for the light nuclei considered in Fig. 2 (see Supplementary Fig. 9 for results obtained with NNLO$_{\rm sat}$ and NN-N^{3}LO + 3N$_{\rm lnl}$). The case of ^{10}C is special because the computed Gamow–Teller transition is very sensitive to the structure of the $J^\pi = 1^+$ state in the ^{10}B daughter nucleus. Depending on the employed interaction, this state can mix with a higher-lying 1^+ state, greatly impacting the precise value of this transition. We finally note that benchmark calculations between the many-body methods used in this work agree to within 5% for the large transition in ^{14}O. For smaller transitions discrepancies can be larger (see Supplementary Information for details).

Historically, the most extensive evidence for the quenching of Gamow–Teller β-decay strength comes from medium-mass nuclei[14,16,27], and we now show that our calculations with these consistent Hamiltonians and currents largely solve the puzzle here as well. We use the valence-space in-medium similarity renormalization group (VS-IMSRG) method[8] (see Methods for details) and compute Gamow–Teller decays for nuclei in the mass range between oxygen and calcium (referred to as *sd*-shell nuclei) and between calcium and vanadium (lower *pf*-shell nuclei), focusing on strong transitions. Here, we highlight the NN-N^{4}LO + 3N$_{\rm lnl}$ interaction and corresponding 2BCs.

Figure 3 shows the empirical values of the Gamow–Teller transition matrix elements versus the corresponding unquenched theoretical matrix elements obtained from the phenomenological shell model with the standard Gamow–Teller $\sigma\tau$ operator and the first-principles VS-IMSRG calculations. Perfect agreement between theory and experiment is denoted by the diagonal dashed line. The results from the phenomenological shell model clearly exemplify the state of theoretical calculations for decades[13–16,27]; as an example, in the *sd*-shell shell, a quenching factor of $q \approx 0.8$ is needed to bring the theory into agreement with experiment[14]. The VS-IMSRG calculations without 2BCs (not shown) exhibit a modest improvement, with a corresponding quenching factor of 0.89(4) for *sd*-shell nuclei and 0.85(3) for *pf*-shell nuclei, pointing to the importance of consistent valence-space wavefunctions and operators (Supplementary Fig. 10). As in ^{100}Sn, the inclusion of 2BCs yields an additional quenching of the theoretical matrix elements, and the linear fit of our results lies close to the dashed line, meaning our theoretical predictions agree, on average, with experimental values across a large number of medium-mass nuclei.

Another approach often used in the investigation of Gamow–Teller quenching is the Ikeda sum-rule: the difference between the total integrated β^- and β^+ strengths obtained with the $\sigma\tau^\mp$ operator yields the model-independent sum-rule $3(N-Z)$. We have computed the Ikeda sum-rule for ^{14}O, ^{48}Ca and ^{90}Zr using the coupled-cluster method (see Methods for details). For the family of EFT Hamiltonians used for ^{100}Sn we obtain a quenching factor arising from 2BCs that is consistent with our results shown in Fig. 3 and the shell-model analyses from refs. [14–16,27]. (Supplementary Fig. 7). We note that the comparison with experimental sum-rule tests using charge-exchange reactions[28,29] is complicated by the use of a hadronic probe, which only corresponds to the leading weak one-body operator, and by the challenge of extracting all strength to high energies. Here, our developments enable future direct comparisons.

It is the combined proper treatment of strong nuclear correlations with powerful quantum many-body solvers and the consistency between 2BCs and three-nucleon forces that largely explains the quenching puzzle. Smaller corrections are still expected to arise from neglected higher-order contributions to currents and Hamiltonians in the EFT approach we pursued, and from neglected correlations in the nuclear wavefunctions. For beyond-standard-model searches of new physics such as neutrino-less double-β-decay, our work suggests that a complete and consistent calculation without a phenomenological quenching of the axial-vector coupling $g_{\rm A}$ is called for. This Letter opens the door to ab initio calculations of weak interactions across the nuclear chart and in stars.

Online content

Any methods, additional references, Nature Research reporting summaries, source data, statements of data availability and associated accession codes are available at https://doi.org/10.1038/s41567-019-0450-7.

Received: 20 April 2018; Accepted: 30 January 2019;
Published online: 11 March 2019

References

1. Janka, H.-T., Langanke, K., Marek, A., Martínez-Pinedo, G. & Müller, B. Theory of core-collapse supernovae. *Phys. Rep.* **442**, 38–74 (2007).
2. Schatz, H. et al. Strong neutrino cooling by cycles of electron capture and β-decay in neutron star crusts. *Nature* **505**, 62–65 (2013).
3. Engel, J. & Menéndez, J. Status and future of nuclear matrix elements for neutrinoless double-beta decay: a review. *Rep. Prog. Phys.* **80**, 046301 (2017).
4. Towner, I. S. Quenching of spin matrix elements in nuclei. *Phys. Rep.* **155**, 263–377 (1987).
5. Epelbaum, E., Hammer, H.-W. & Meißner, U.-G. Modern theory of nuclear forces. *Rev. Mod. Phys.* **81**, 1773–1825 (2009).
6. Barrett, B. R., Navrátil, P. & Vary, J. P. Ab initio no core shell model. *Prog. Part. Nucl. Phys.* **69**, 131–181 (2013).
7. Hagen, G. et al. Neutron and weak-charge distributions of the ^{48}Ca nucleus. *Nat. Phys.* **12**, 186–190 (2016).
8. Stroberg, S. R. et al. Nucleus-dependent valence-space approach to nuclear structure. *Phys. Rev. Lett.* **118**, 032502 (2017).
9. Korobkin, O., Rosswog, S., Arcones, A. & Winteler, C. On the astrophysical robustness of the neutron star merger *r*-process. *Mon. Not. R. Astron. Soc.* **426**, 1940–1949 (2012).
10. Mumpower, M. R., Surman, R., McLaughlin, G. C. & Aprahamian, A. The impact of individual nuclear properties on *r*-process nucleosynthesis. *Prog. Part. Nucl. Phys.* **86**, 86–126 (2016).
11. Pian, E. et al. Spectroscopic identification of *r*-process nucleosynthesis in a double neutron-star merger. *Nature* **551**, 67–70 (2017).
12. Barea, J., Kotila, J. & Iachello, F. Limits on neutrino masses from neutrinoless double-β decay. *Phys. Rev. Lett.* **109**, 042501 (2012).
13. Wilkinson, D. H. Renormalization of the axial-vector coupling constant in nuclear β-decay (II). *Nucl. Phys. A* **209**, 470–484 (1973).
14. Brown, B. A. & Wildenthal, B. H. Experimental and theoretical Gamow–Teller beta-decay observables for the *sd*-shell nuclei. *At. Data Nucl. Data Tables* **33**, 347–404 (1985).
15. Chou, W.-T., Warburton, E. K. & Brown, B. A. Gamow–Teller beta-decay rates for $A \leq 18$ nuclei. *Phys. Rev. C* **47**, 163–177 (1993).
16. Martínez-Pinedo, G., Poves, A., Caurier, E. & Zuker, A. P. Effective G_A in the *pf* shell. *Phys. Rev. C* **53**, R2602–R2605 (1996).
17. Machleidt, R. & Entem, D. R. Chiral effective field theory and nuclear forces. *Phys. Rep.* **503**, 1–75 (2011).
18. Holt, J. W., Kaiser, N. & Weise, W. Chiral three-nucleon interaction and the ^{14}C-dating β decay. *Phys. Rev. C* **79**, 054331 (2009).
19. Maris, P. et al. Origin of the anomalous long lifetime of ^{14}C. *Phys. Rev. Lett.* **106**, 202502 (2011).
20. Hinke, C. B. et al. Superallowed Gamow–Teller decay of the doubly magic nucleus ^{100}Sn. *Nature* **486**, 341–345 (2012).
21. Morris, T. D. et al. Structure of the lightest tin isotopes. *Phys. Rev. Lett.* **120**, 152503 (2018).
22. Hebeler, K., Bogner, S. K., Furnstahl, R. J., Nogga, A. & Schwenk, A. Improved nuclear matter calculations from chiral low-momentum interactions. *Phys. Rev. C* **83**, 031301 (2011).
23. Ekström, A. et al. Accurate nuclear radii and binding energies from a chiral interaction. *Phys. Rev. C* **91**, 051301 (2015).
24. Leistenschneider, E. et al. Dawning of the $N=32$ shell closure seen through precision mass measurements of neutron-rich titanium isotopes. *Phys. Rev. Lett.* **120**, 062503 (2018).
25. Batist, L. et al. Systematics of Gamow–Teller beta decay 'southeast' of ^{100}Sn. *Eur. Phys. J. A* **46**, 45–53 (2010).
26. Pastore, S. et al. Quantum Monte Carlo calculations of weak transitions in $A=6$–10 nuclei. *Phys. Rev. C* **97**, 022501 (2018).
27. Langanke, K., Dean, D. J., Radha, P. B., Alhassid, Y. & Koonin, S. E. Shell-model Monte Carlo studies of *fp*-shell nuclei. *Phys. Rev. C* **52**, 718–725 (1995).
28. Gaarde, C. et al. Excitation of giant spin–isospin multipole vibrations. *Nucl. Phys. A* **369**, 258–280 (1981).
29. Wakasa, T. et al. Gamow–Teller strength of ^{90}Nb in the continuum studied via multipole decomposition analysis of the ^{90}Zr(*p*,*n*) reaction at 295 MeV. *Phys. Rev. C* **55**, 2909–2922 (1997).
30. Bhat, M. R. in Qaim, S. M. (ed.) *Nuclear Data for Science and Technology*, 817 (Springer, Berlin, 1992).
31. Brown, B. A. & Richter, W. A. New 'USD' Hamiltonians for the *sd* shell. *Phys. Rev. C* **74**, 034315 (2006).

Acknowledgements

The authors thank H. Grawe and T. Faestermann for useful correspondence, J. Engel, E. Epelbaum, D. Gazit, H. Krebs, D. Lubos, S. Pastore and R. Schiavilla for useful discussions and K. Hebeler for providing us with matrix elements in Jacobi coordinates for the three-nucleon interaction at next-to-next-to-leading order[22]. This work was prepared in part by Lawrence Livermore National Laboratory (LLNL) under contract DE-AC52-07NA27344 and was supported by the Office of Nuclear Physics, US Department of Energy, under grants DE-FG02-96ER40963, DE-FG02-97ER41014, DE-SC0008499, DE-SC0018223 and DE-SC0015376, the Field Work Proposals ERKBP57 and ERKBP72 at Oak Ridge National Laboratory (ORNL), the FWP SCW1579, LDRD projects 18-ERD-008 and 18-ERD-058 and the Lawrence Fellowship Program at LLNL, and by NSERC grant no. SAPIN-2016-00033, ERC grant no. 307986 STRONGINT and the DFG under grant SFB 1245. TRIUMF receives federal funding through a contribution agreement with the National Research Council of Canada. Computer time was provided by the Innovative and Novel Computational Impact on Theory and Experiment (INCITE) programme. This research used resources of the Oak Ridge Leadership Computing Facility located at ORNL, which is supported by the Office of Science of the Department of Energy under contract no. DE-AC05-00OR22725. Computations were also performed at LLNL Livermore Computing under the institutional Computing Grand Challenge Program, at Calcul Quebec, Westgrid and Compute Canada, and at the Jülich Supercomputing Center (JURECA).

Author contributions

G.H., T.D.M. and T.P. performed the coupled-cluster calculations. G.R.J. computed three-nucleon forces for the coupled-cluster calculations. P.G., S.Q., P.N. and K.A.W. performed calculations for the two-body currents. P.N. developed the higher-precision chiral three-nucleon interactions used in this work and performed no-core shell model calculations. G.H. and T.D.M. derived and implemented the new formalism to incorporate higher-order excitations in coupled-cluster theory. S.R.S. and J.D.H. performed VS-IMSRG calculations. All authors discussed the results and contributed to the manuscript at all stages.

Competing interests

The authors declare no competing interests.

Additional information

Supplementary information is available for this paper at https://doi.org/10.1038/s41567-019-0450-7.

Reprints and permissions information is available at www.nature.com/reprints.

Correspondence and requests for materials should be addressed to G.H.

Journal Peer Review Information: *Nature Physics* thanks Norbert Kaiser and other anonymous reviewer(s) for their contribution to the peer review of this work.

Publisher's note: Springer Nature remains neutral with regard to jurisdictional claims in published maps and institutional affiliations.

Methods

Hamiltonians and model space. In this work we employ the intrinsic Hamiltonian

$$H=\sum_{i<j}\left(\frac{(p_i-p_j)^2}{2mA}+V_{\rm NN}^{(i,j)}\right)+\sum_{i<j<k}V_{\rm 3N}^{(i,j,k)} \quad (1)$$

Here p_i is the nucleon momentum, m the average nucleon mass, A the mass number of the nucleus of interest, $V_{\rm NN}$ the nucleon–nucleon (NN) interaction and $V_{\rm 3N}$ the three-nucleon (3N) interaction.

We use a set of interactions from ref. [22] labelled 1.8/2.0 (EM), 2.0/2.0 (EM), 2.2/2.0 (EM), 2.8/2.0 (EM) and 2.0/2.0 (PWA). These consist of a chiral NN interaction at order N^{3}LO from ref. [32] evolved to the resolution scales $\lambda_{\rm SRG}=1.8$, 2.0, 2.2 and 2.8 fm^{-1} by means of the similarity renormalization group (SRG)[33] plus a chiral 3N interaction (unevolved) at order N^{2}LO, using a non-local regulator with momentum cutoff $\Lambda_{\rm 3N}=2.0$ fm^{-1}. Note that the 2.0/2.0 (PWA) interaction employs different long-range pion couplings in the NN and 3N sectors. The low-energy couplings entering these interactions were adjusted to reproduce NN scattering data as well as the ^{3}H binding energy and ^{4}He charge radius. With the exception of 2.8/2.0 (EM), this set of interactions was recently used to describe binding energies and spectra of neutron-rich nuclei up to ^{78}Ni (refs. [34,35]) and of neutron-deficient nuclei around ^{100}Sn (ref. [21]). The results with the 1.8/2.0 (EM) interaction, in particular, reproduce ground-state energies very well.

In addition, we also employ the NNLO$_{\rm sat}$ interaction, which was constrained to reproduce nuclear binding energies and charge radii of selected p- and sd-shell nuclei[23]. Ab initio calculations based on NNLO$_{\rm sat}$ accurately describe both the radii and binding energies of light- and medium-mass nuclei[7].

Finally, we employ two consistently SRG-evolved NN and 3N interactions, namely NN-N^{3}LO + 3N$_{\rm lnl}$ (ref. [24]) and the NN-N^{4}LO + 3N$_{\rm lnl}$ introduced in this work. The NN interactions at N^{3}LO and N^{4}LO are from refs. [32,36], respectively. The 3N interactions 3N$_{\rm lnl}$ use a mixture of local[37] and non-local regulators. The local cutoff is 650 MeV and the non-local cutoff of 500 MeV is the same as in the NN interactions. In the case of the NN-N^{4}LO + 3N$_{\rm lnl}$, the parameters of the two-pion-exchange 3N forces (c_1, c_3 and c_4) are shifted with respect to their values in the NN potential following the recommendation of ref. [36]. The couplings of the shorter-range 3N forces ($c_{\rm D}$ and $c_{\rm E}$) are constrained to the binding energies and radii of the triton and ^{4}He in the NN-N^{3}LO + 3N$_{\rm lnl}$ model, and to the triton half-life and binding energy in the NN-N^{4}LO + 3N$_{\rm lnl}$ model. We note, however, that the NN-N^{3}LO + 3N$_{\rm lnl}$ interaction also reproduces the triton half-life as shown in Supplementary Fig. 9. The NN and 3N interactions are consistently SRG evolved to the lower cutoff $\lambda_{\rm SRG}=2.0$ fm^{-1} (or $\lambda_{\rm SRG}=1.8$ fm^{-1} in the case of some of our light-nuclei calculations).

In our NCSM calculations of light nuclei we employ the harmonic-oscillator basis varied in the range $N_{\rm max}=4$–14 and with frequency $\hbar\omega=20$ MeV. In our coupled-cluster and VS-IMSRG calculations we start from a Hartree–Fock basis built from the harmonic-oscillator basis with model-space parameters in the range $N_{\rm max}=6$–14 and $\hbar\omega=12$–16 MeV, respectively. Finally, the 3N interaction is truncated to three-particle energies with $E_{\rm 3max}\leq 16\hbar\omega$.

Gamow–Teller transition operator. The rate at which a Gamow–Teller transition will occur is proportional to the square of the reduced transition matrix element

$$M_{\rm GT}=\langle f\,||O_{\rm GT}||\,i\rangle \quad (2)$$

Here, i and f label the initial and final states of the mother and daughter nuclei, respectively. (Note that, throughout this work, we quote the reduced matrix element $\langle f\,||O_{\rm GT}||\,i\rangle$, using the Edmonds convention[38]). The transition operator $O_{\rm GT}$ is defined in terms of the $J=1$ transverse electric multipole of the charge-changing axial-vector current[39] $\mathbf{J}^A(\vec{\mathbf{K}})$

$$O_{\rm GT}=g_{\rm A}^{-1}\sqrt{6\pi}\,E_1^A(\mathbf{K}=0) \quad (3)$$

Here, $\mathbf{K}$ denotes the momentum transferred to the resulting electron and anti-neutrino pair (or positron and neutrino in β^+-decay). Because the change in energy between mother and daughter states is typically very small (a few MeV) compared to other relevant scales, setting $|\mathbf{K}|=0$ is a very good approximation that significantly simplifies the calculation of $M_{\rm GT}$.

The standard (one-body) charge-changing axial-vector current is given by

$$\mathbf{J}^A(\mathbf{K})=\sum_j ig_A\sigma_j\tau_j^{\pm}e^{i\mathbf{K}\cdot\mathbf{r}_j} \quad (4)$$

Here $\mathbf{r}_j$, σ_j, $\tau_j^{\pm}$ are the position, Pauli spin and charge-raising (lowering) operators for the jth particle. In this work we use axial-vector currents derived within the same chiral EFT framework used for the strong interactions, including the leading 2BC[40]. For a diagrammatic picture of the relevant contributions (at $\mathbf{K}=0$) see Supplementary Fig. 5. The leftmost diagram corresponds to the leading-order one-body current. In addition, we include two classes of 2BC: a short-range term that shares a parameter ($c_{\rm D}$) with the one-pion-exchange 3N force, as well as two long-range terms that share parameters (c_3 and c_4) with the two-pion-exchange NN and 3N forces. Within this framework, the Gamow–Teller operator naturally decomposes into two major terms, the standard one-body current ($O_{\sigma\tau}^{1b}=\sigma\tau^{\pm}$) and a 2BC:

$$O_{\rm GT}=O_{\sigma\tau}^{1b}+O_{\rm 2BC}^{2b} \quad (5)$$

For each of the chiral EFT Hamiltonians employed in this work, the parameters $c_{\rm D}$, c_3 and c_4 are taken consistently in the 3N force and 2BC, and the momentum cutoff for the regularization of the currents, $\Lambda_{\rm 2BC}$, is set to the value used in the non-local regulator of the 3N interaction (Supplementary Table 2). We found that the choice of a local[41] versus non-local regulator in the 2BC has a negligible effect on the Gamow–Teller transition strength. The majority of our results were obtained using a local regulator. When appropriate, the currents were consistently evolved with the nuclear forces to a lower resolution using the SRG (for NN-N^{3}LO + 3N$_{\rm lnl}$ and NN-N^{4}LO + 3N$_{\rm lnl}$), keeping only up to two-body contributions. In light nuclei, three- and higher-body SRG-induced terms are very small.

Quantum many-body methods. In what follows we describe the many-body methods used in this work: coupled-cluster theory, the NCSM and the IMSRG. The coupled-cluster calculations required new methodological developments, which are described in detail below.

Coupled-cluster method. Our coupled-cluster calculations start from a Hamiltonian H_N that is normal-ordered with respect to a single-reference Hartree-Fock state $|\Phi_0\rangle$. We approximate the full 3N interaction by truncating it at the normal-ordered two-body level. This approximation has been shown to work well for light- and medium-mass nuclei[42–44]. The central quantity in the coupled-cluster method is the similarity transformed Hamiltonian $\overline{H}_N=e^{-T}H_Ne^T$, with $T=T_1+T_2+\ldots$ being a linear expansion of particle–hole excitations with respect to the reference state $|\Phi_0\rangle$. The truncation of this expansion at some low-order particle–hole excitation rank is the only approximation that occurs in the coupled-cluster method[45,46]. The non-Hermitian Hamiltonian $\overline{H}_N$ is correlated and the reference state $|\Phi_0\rangle$ becomes the exact ground state.

We compute ground and excited states using the CCSDT-1 and EOM-CCSDT-1 approximations[47,48], respectively. These approximations include iterative singles and doubles and leading-order triples excitations, and capture ~99% of the correlation energy in closed (sub-) shell systems[4]. For the Gamow–Teller transitions and expectation values, we solve for the left ground state of $\overline{H}_N$:

$$\langle\Phi_0|(1+\Lambda),\quad \text{with}\quad \Lambda=\Lambda_1+\Lambda_2+\ldots \quad (6)$$

Here, Λ is a linear expansion in particle–hole de-excitation operators. We truncate Λ at the EOM-CCSDT-1 level consistent with the right CCSDT-1 ground-state solution[48].

The Gamow–Teller transition of a $J^\pi=0^+$ ground state occupies low-lying 1^+ states in the daughter nucleus. These states in the daughter nucleus are calculated by employing the charge-exchange equation-of-motion coupled-cluster method[49], and we also include the leading-order three-particle–three-hole excitations as defined by the EOM-CCSDT-1 approximation[48]. The absolute squared Gamow–Teller transition matrix element is then

$$\begin{aligned}|M_{\rm GT}|^2 &= |\langle f|O_{\rm GT}|i\rangle|^2=\langle f\,|O_{\rm GT}|\,i\rangle\langle i\,|O_{\rm GT}^\dagger|\,f\rangle\\ &= \langle\Phi_0\,|L_\mu^{1^+}\overline{O_N}|\,\Phi_0\rangle\langle\Phi_0\,|(1+\Lambda)\,\overline{O_N^\dagger}R_\mu^{1^+}|\,\Phi_0\rangle\end{aligned} \quad (7)$$

Here, $R_\mu^{1^+}$ is the right and $L_\mu^{1^+}$ the corresponding left excited 1^+ state in the daughter nucleus, and $\overline{O_N}=e^{-T}O_Ne^T$ is the similarity transform of the normal-ordered Gamow–Teller operator $O_{\rm GT}$ (equation (5)). In O_N we approximate the two-body part of the operator $O_{\rm GT}$ at the normal-ordered one-body level, neglecting the residual two-body normal-ordered part[49,50]. Note that the construction of $\overline{O_N}$ induces higher-body terms, and we truncate $\overline{O_N}$ at the two-body level. This approximation is precise for the case of electromagnetic sum-rules in coupled-cluster theory[51].

We evaluate the total integrated Gamow–Teller strengths as a ground-state expectation value

$$S^{\pm}=\langle\Phi_0|(1+\Lambda)\,\overline{O_N^\dagger}\cdot\overline{O_N}|\Phi_0\rangle \quad (8)$$

For $O=O_{\sigma\tau}^{1b}$ the Ikeda sum-rule is $S^- - S^+ = 3(N-Z)$ (refs. [52,53]). As a check of our code, we have verified that this sum-rule is fulfilled.

The inclusion of triples excitations of the right and left eigenstates R_μ and L_μ, respectively, is challenging in terms of CPU time and memory. To limit CPU time, we restrict the employed three-particle–three-hole configurations in the EOM-CCSDT-1 calculations to the vicinity of the Fermi surface. This is done by introducing a single-particle index $\tilde{e}_p=|N_p-N_{\rm F}|$ that measures the difference between the numbers of oscillator shells N_p of the single-particle state with respect to the Fermi surface $N_{\rm F}$. We only allow three-particle and three-hole configurations with $\tilde{E}_{pqr}=\tilde{e}_p+\tilde{e}_q+\tilde{e}_r<\tilde{E}_{\rm 3max}$. This approach yields a rapid convergence in EOM-CCSDT-1 calculations, as seen in Supplementary Fig. 12.

The storage of the included three-particle–three-hole amplitudes exceeds currently available resources and had to be avoided. We follow ref. [54] and define an effective Hamiltonian in the P space of singles and doubles excitations, so that no explicit triples amplitudes need be stored. Denoting the Q-space as that of all triples excitations below $\tilde{E}_{3\mathrm{max}}$, the right eigenvalue equation can be rewritten as

$$\begin{bmatrix} \overline{H}_{PP} & \overline{H}_{PQ} \\ \overline{H}_{QP} & \overline{H}_{QQ} \end{bmatrix} \begin{bmatrix} R_P \\ R_Q \end{bmatrix} = \omega \begin{bmatrix} R_P \\ R_Q \end{bmatrix} \tag{9}$$

This yields

$$\overline{H}_{PP}R_P + \overline{H}_{PQ}R_Q = \omega R_P \tag{10}$$

and

$$\overline{H}_{QP}R_P + \overline{H}_{QQ}R_Q = \omega R_Q \tag{11}$$

Here, we have suppressed the label μ denoting different excited states. Solving equation (11) for the triples component of R, and then substituting into equation (10), we arrive at

$$\overline{H}_{PP}R_P + \overline{H}_{PQ}(\omega - \overline{H}_{QQ})^{-1}\overline{H}_{QP}R_P = \omega R_P \tag{12}$$

In the EOM-CCSDT-1 approximation $\overline{H}_{QQ} = \langle T|F|T\rangle$, where F is the Fock matrix. In the Hartree–Fock basis $\overline{H}_{QQ}$ is diagonal, and its inversion is trivial. We solve this energy-dependent, effective Hamiltonian self-consistently to arrive at exact eigenstates of the EOM-CCSDT-1 Hamiltonian. This allows for only one state to be constructed at a time. For the computation of higher spin excited states in the daughter nucleus ^{100}In (ref. [55]), we combine the iterative EOM-CCSDT-1 approach, with a perturbative approach that accounts for all excluded three-particle–three-excitations outside the energy cut $\tilde{E}_{3\mathrm{max}}$. This approach is analogous to the active space coupled cluster methods of refs. [56,57]. By denoting the Q'-space as that of all three-particle–three-hole excitations above $\tilde{E}_{3\mathrm{max}}$, we arrive at the following perturbative non-iterative energy correction:

$$\Delta\omega_\mu = \langle \Phi_0 | L_\mu \overline{H}_{PQ'}(\omega_\mu - \overline{H}_{Q'Q'})^{-1}\overline{H}_{Q'P}R_\mu | \Phi_0 \rangle \tag{13}$$

Here, R_μ and L_μ are the right and corresponding left EOM-CCSDT-1 eigenstates obtained from diagonalization of the energy-dependent similarity transformed Hamiltonian given in equation (12). We label this approach EOM-CCSDt-1, and it drastically improves convergence to the full-space EOM-CCSDT-1 energies (see Supplementary Fig. 15 for details).

NCSM. The NCSM[6,58] treats nuclei as systems of A non-relativistic point-like nucleons interacting through realistic inter-nucleon interactions. All nucleons are active degrees of freedom. The many-body wavefunction is cast into an expansion over a complete set of antisymmetric A-nucleon harmonic-oscillator basis states containing up to N_{max} harmonic-oscillator excitations above the lowest Pauli-principle-allowed configuration:

$$|\Psi_A^{J^\pi T}\rangle = \sum_{N=0}^{N_{\mathrm{max}}} \sum_i c_{Ni}^{J^\pi T} |ANiJ^\pi T\rangle \tag{14}$$

Here, N denotes the total number of harmonic-oscillator excitations of all nucleons above the minimum configuration, $J^\pi T$ are the total angular momentum, parity and isospin, and i denotes additional quantum numbers. The sum over N is restricted by parity to either an even or odd sequence. The basis is further characterized by the frequency ω of the harmonic oscillator. Square-integrable energy eigenstates are obtained by diagonalizing the intrinsic Hamiltonian, typically by applying the Lanczos algorithm. In the present work we used the importance-truncation NCSM[59] to reduce the basis size in the highest N_{max} spaces of the $A = 10$ and $A = 14$ nucleus calculations.

VS-IMSRG. The IMSRG[60,61] transforms the many-body Hamiltonian H to a diagonal or block-diagonal form via a unitary transformation U; that is, it generates $\widetilde{H} = UHU^\dagger$. To achieve this, one expresses the transformation as the exponential of an anti-Hermitian generator, $U = e^\Omega$. Here, Ω encodes information on the off-diagonal physics to be decoupled[62]. Beginning from some single-reference ground-state configuration $|\Phi_0\rangle$ (for example, the Hartree–Fock state based on initial interactions), we map the reference to the fully correlated ground state $|\Psi_0\rangle$ via a continuous sequence of such unitary transformations $U(s)$. With no approximations, this gives the exact ground-state energy, but in the IMSRG(2) approximation used here, all operators are truncated at the two-body level.

In the valence-space formulation, VS-IMSRG[8,63], the unitary transformation is constructed (based on a redefinition of Ω) to also decouple a valence-space Hamiltonian H_{vs} from the remainder of the Hilbert space. We use an ensemble reference[8] state for normal ordering to capture the main effects of three-body operators within the valence space. The eigenstates are obtained by a subsequent diagonalization of H_{vs} within the valence space. Furthermore, any general operator $\mathcal{O}$ can then be transformed by $\widetilde{\mathcal{O}} = e^\Omega \mathcal{O} e^{-\Omega}$, to produce an effective valence-space operator consistent with the valence-space Hamiltonian[64]. The expectation value of $\mathcal{O}$ between initial and final states is obtained as usual by combining the matrix elements of $\mathcal{O}$ with the one- and two-body shell-model transition densities. Note that there is some ambiguity about which reference we should take when normal ordering: the parent or the daughter. If we were able to perform the unitary transformation without approximation, either choice should give exactly the same answer, as long as we use the same transformation on the wavefunctions and the operators. However, because we truncate at the two-body level, the transformation is not unitary and the error made is reference-dependent. Comparing results obtained by normal ordering with respect to the parent or the daughter nucleus then provides a (lower bound) estimate of the error due to the truncation. In this work, we find that the different choices give transition matrix elements that differ on the order of ~5%. The results presented are those obtained with the parent as the reference. As an example, if we use ^{14}N as the reference, the numbers in the third line of Supplementary Table 4 become 1.77, 1.81, 1.88 and 1.87 (refs. [65,66]).

Data availability

The data that support the plots within this paper and other findings of this study are available from the corresponding author upon reasonable request.

References

32. Entem, D. R. & Machleidt, R. Accurate charge-dependent nucleon–nucleon potential at fourth order of chiral perturbation theory. *Phys. Rev. C* **68**, 041001 (2003).
33. Bogner, S. K., Furnstahl, R. J. & Perry, R. J. Similarity renormalization group for nucleon–nucleon interactions. *Phys. Rev. C* **75**, 061001 (2007).
34. Hagen, G., Jansen, G. R. & Papenbrock, T. Structure of ^{78}Ni from first-principles computations. *Phys. Rev. Lett.* **117**, 172501 (2016).
35. Simonis, J., Stroberg, S. R., Hebeler, K., Holt, J. D. & Schwenk, A. Saturation with chiral interactions and consequences for finite nuclei. *Phys. Rev. C* **96**, 014303 (2017).
36. Entem, D. R., Machleidt, R. & Nosyk, Y. High-quality two-nucleon potentials up to fifth order of the chiral expansion. *Phys. Rev. C* **96**, 024004 (2017).
37. Navrátil, P. Local three-nucleon interaction from chiral effective field theory. *Few-Body Systems* **41**, 117–140 (2007).
38. Edmonds, A. R. *Angular Momentum in Quantum Mechanics* (Princeton Univ. Press, Princeton, NJ, 1957).
39. Krebs, H., Epelbaum, E. & Meißner, U.-G. Nuclear axial current operators to fourth order in chiral effective field theory. *Ann. Phys.* **378**, 317–395 (2017).
40. Park, T.-S. et al. Parameter-free effective field theory calculation for the solar proton-fusion and hep processes. *Phys. Rev. C* **67**, 055206 (2003).
41. Gazit, D., Quaglioni, S. & Navrátil, P. Three-nucleon low-energy constants from the consistency of interactions and currents in chiral effective field theory. *Phys. Rev. Lett.* **103**, 102502 (2009).
42. Hagen, G. et al. Coupled-cluster theory for three-body Hamiltonians. *Phys. Rev. C* **76**, 034302 (2007).
43. Roth, R. et al. Medium-mass nuclei with normal-ordered chiral $NN+3N$ interactions. *Phys. Rev. Lett.* **109**, 052501 (2012).
44. Hergert, H. et al. In-medium similarity renormalization group with chiral two- plus three-nucleon interactions. *Phys. Rev. C* **87**, 034307 (2013).
45. Bartlett, R. J. & Musiał, M. Coupled-cluster theory in quantum chemistry. *Rev. Mod. Phys.* **79**, 291–352 (2007).
46. Hagen, G., Papenbrock, T., Hjorth-Jensen, M. & Dean, D. J. Coupled-cluster computations of atomic nuclei. *Rep. Prog. Phys.* **77**, 096302 (2014).
47. Lee, Y. S., Kucharski, S. A. & Bartlett, R. J. A coupled cluster approach with triple excitations. *J. Chem. Phys.* **81**, 5906–5912 (1984).
48. Watts, J. D. & Bartlett, R. J. Economical triple excitation equation-of-motion coupled-cluster methods for excitation energies. *Chem. Phys. Lett.* **233**, 81–87 (1995).
49. Ekström, A. et al. Effects of three-nucleon forces and two-body currents on Gamow–Teller strengths. *Phys. Rev. Lett.* **113**, 262504 (2014).
50. Menéndez, J., Gazit, D. & Schwenk, A. Chiral two-body currents in nuclei: Gamow–Teller transitions and neutrinoless double-beta decay. *Phys. Rev. Lett.* **107**, 062501 (2011).
51. Miorelli, M., Bacca, S., Hagen, G. & Papenbrock, T. Computing the dipole polarizability of ^{48}Ca with increased precision. *Phys. Rev. C* **98**, 014324 (2018).
52. Ikeda, K., Fujii, S. & Fujita, J. The (p,n) reactions and beta decays. *Phys. Lett.* **3**, 271–272 (1963).
53. Yako, K. et al. Gamow–Teller strength distributions in ^{48}Sc by the ^{48}Ca(p,n) and ^{48}Ti(n,p) reactions and two-neutrino double-β decay nuclear matrix elements. *Phys. Rev. Lett.* **103**, 012503 (2009).
54. Smith, C. E., King, R. A. & Crawford, T. D. Coupled cluster methods including triple excitations for excited states of radicals. *J. Chem. Phys.* **122**, 054110 (2005).

55. Faestermann, T., Górska, M. & Grawe, H. The structure of ^{100}Sn and neighbouring nuclei. *Prog. Part. Nucl. Phys.* **69**, 85–130 (2013).
56. Shen, J. & Piecuch, P. Biorthogonal moment expansions in coupled-cluster theory: review of key concepts and merging the renormalized and active-space coupled-cluster methods. *Chem. Phys.* **401**, 180–202 (2012).
57. Shen, J. & Piecuch, P. Combining active-space coupled-cluster methods with moment energy corrections via the CC(*P*;*Q*) methodology, with benchmark calculations for biradical transition states. *J. Chem. Phys.* **136**, 144104 (2012).
58. Navrátil, P., Vary, J. P. & Barrett, B. R. Large-basis ab initio no-core shell model and its application to ^{12}C. *Phys. Rev. C* **62**, 054311 (2000).
59. Roth, R. & Navrátil, P. Ab Initio study of ^{40}Ca with an importance-truncated no-core shell model. *Phys. Rev. Lett.* **99**, 092501 (2007).
60. Tsukiyama, K., Bogner, S. K. & Schwenk, A. In-medium similarity renormalization group for nuclei. *Phys. Rev. Lett.* **106**, 222502 (2011).
61. Hergert, H., Bogner, S. K., Morris, T. D., Schwenk, A. & Tsukiyama, K. The in-medium similarity renormalization group: a novel ab initio method for nuclei. *Phys. Rep.* **621**, 165–222 (2016).
62. Morris, T. D., Parzuchowski, N. M. & Bogner, S. K. Magnus expansion and in-medium similarity renormalization group. *Phys. Rev. C* **92**, 034331 (2015).
63. Bogner, S. K. et al. Nonperturbative shell-model interactions from the in-medium similarity renormalization group. *Phys. Rev. Lett.* **113**, 142501 (2014).
64. Parzuchowski, N. M., Stroberg, S. R., Navrátil, P., Hergert, H. & Bogner, S. K. Ab initio electromagnetic observables with the in-medium similarity renormalization group. *Phys. Rev. C* **96**, 034324 (2017).
65. Brown, B. A. & Wildenthal, B. H. Status of the nuclear shell model. *Annu. Rev. Nucl. Part. Sci.* **38**, 29–66 (1988).
66. Wildenthal, B. H., Curtin, M. S. & Brown, B. A. Predicted features of the beta decay of neutron-rich *sd*-shell nuclei. *Phys. Rev. C* **28**, 1343–1366 (1983).